nature catalysis

ARTICLES

https://doi.org/10.1038/s41929-020-00520-x

Check for updates

Acidity of surface-infiltrated binary oxides as a sensitive descriptor of oxygen exchange kinetics in mixed conducting oxides

Clement Nicollet[1,5]✉, Cigdem Toparli[2], George F. Harrington[1,3,4], Thomas Defferriere[1], Bilge Yildiz[1,2] and Harry L. Tuller[1,3]

Improving the kinetics of O_2 reduction on oxide surfaces is critical in many energy and fuel conversion technologies. Here we show that the acidity scale for binary oxides is a powerful descriptor for tuning and predicting oxygen surface exchange kinetics on mixed conducting oxides. By infiltrating a selection of binary oxides from strongly basic (Li_2O) to strongly acidic (SiO_2) onto the surface of $Pr_{0.1}Ce_{0.9}O_{2-\delta}$ samples, it was possible to vary the chemical surface exchange coefficient k_{chem} by 6 orders of magnitude, with basic oxides such as Li_2O increasing k_{chem} by nearly 1,000 times, with surface concentrations as low as 50 ppm impacting k_{chem}. Strikingly, although the pre-exponential of k_{chem} scales linearly with the acidity of the infiltrated binary oxide, there is nearly no change in the activation energy. The origin of these dramatic changes is proposed to arise from the systematic increase in electron concentration at the $Pr_{0.1}Ce_{0.9}O_{2-\delta}$ surface with the decreasing acidity of the infiltrated binary oxide.

The ability of metal oxides to support both electronic and ionic conductivity, as well as their inherent thermal and chemical stability, make them attractive for applications that range from energy conversion and storage devices (solid oxide fuel cells, electrolysers, permeation membranes, high-energy-density batteries and photothermal reactors)[1–5], automotive emission catalysts and sensors[6–8], and more recently valence-change memory devices[9,10]. In these and other applications, the rate at which oxygen can exchange between the solid and the surrounding gas atmosphere, under various temperatures and oxygen partial pressure excursions, often determines the overall performance of the devices. As a consequence, surface exchange kinetics have been the focus of many studies and reviews, particularly associated with the performance of solid oxide fuel cells/electrolysers, permeation membranes and oxygen storage materials[11]. As important as oxygen surface exchange kinetics are to these technologies, they are often difficult to control and reproduce, even for nominally the same material systems[12–14], and they inevitably degrade with time under operation[15,16].

The reaction of gaseous oxygen on an oxide surface is often described in several steps, from the gas diffusion of molecular oxygen towards the surface, surface adsorption, dissociation of the O_2 molecule into adsorbed O atoms, charge transfer of electrons from the solid to the adsorbed oxygen species, diffusion of the ions towards and subsequent insertion into surface oxygen vacancies, and ionic diffusion inwards from the surface into the bulk. The identity of the rate-limiting factors that control these kinetics, however, remains controversial[11,17–19]. Generally, there is consensus that materials that exhibit mixed ionic and electronic conductivity in the bulk, such as the transition metal perovskites (for example, $(La,Sr)CoO_3$ or $Sr(Ti,Fe)O_3$), the related Ruddlesden–Popper layer compounds (for example, Pr_2NiO_4) and ceria-based fluorites (for example, $(Pr,Ce)O_2$), exhibit considerably higher oxygen exchange rates than materials that are largely either solely electronic conductors (for example, $(La,Sr)MnO_3$) or ionic conductors (for example, $(Zr,Y)O_2$—yttria stabilized zirconia), particularly at reduced temperatures. In many cases, a stronger dependence of the exchange rate on the magnitude of ionic conductivity is demonstrated[20], whereas in other cases a dependence on the magnitude of the electronic conductivity appears to dominate[20,21].

Given that oxygen exchange occurs at the surface of these materials, it is not surprising that its kinetics are found to be sensitive to surface composition and its evolution. Although widely studied, the role of surface species in impacting oxygen exchange kinetics remains controversial and at times contradictory. For example, the segregation of certain cations, notably Sr (refs [22,23]) in the perovskite oxides referenced above, is well-known to degrade the rate of oxygen exchange, apparently by forming a SrO_x layer that acts as a charge-transfer barrier[22]. Indeed, recently Rupp et al. reported that during the in situ surface modification of thin-film $La_{0.6}Sr_{0.4}CoO_{3-\delta}$ cathodes within a pulsed laser deposition chamber, increasing the Sr concentration at the surface systematically decreases the electrical surface exchange coefficient k^q (ref. [24]). Some authors showed, on the contrary, that the addition of Sr to the surface from an external source contributes to enhanced surface exchange kinetics[25,26]. In a particularly notable example, Argirusis and co-workers reported that the exchange rate measured by oxygen $^{18}O/^{16}O$ tracer exchange, followed by secondary-ion mass spectrometry analysis on Fe-doped $SrTiO_3$ single crystals coated with thin films of SrO and BaO, was enhanced by as much as three orders of magnitude compared with that of the same crystal with no coating[27,28]. Other authors showed that the addition of other foreign cations to the surface can have either a positive or negative impact on the oxygen exchange rate[29,30], and relate their effect to an enhanced oxygen-vacancy formation at the surface. Tsvetkov et al.[31], however, came to the

[1]Department of Materials Science and Engineering, Massachusetts Institute of Technology, Cambridge, MA, USA. [2]Department of Nuclear Science and Engineering, Massachusetts Institute of Technology, Cambridge, MA, USA. [3]International Institute of Carbon Neutral Energy Research, Kyushu University, Fukuoka, Japan. [4]Center of Coevolutionary Research for Sustainable Communities (C2RSC), Kyushu University, Fukuoka, Japan. [5]Present address: Université de Nantes, CNRS, Institut des Matériaux Jean Rouxel, IMN, Nantes, France. ✉e-mail: clement.nicollet@cnrs-imn.fr

opposite conclusion, that is, that the addition of an oxide with a lower enthalpy of oxygen-vacancy formation increased both the electrical surface exchange coefficient and its stability. In these studies, the impact of foreign cation additions on the oxygen exchange kinetics was moderate. As the results appear to be contradictory between the studies, it is difficult to establish a trend that aids us to predict whether an additive element will serve to degrade or improve the oxygen exchange kinetics and to what degree. Additionally, a wide spectrum of species that deposit on the surface inadvertently from the environment are reported to have a detrimental impact on the oxygen exchange kinetics[32]. Chromium from metal-based fuel cell interconnects or silica from furnace refractories are known to be quite deleterious, as they considerably reduce the oxygen exchange rate with increasing operating time and, as a consequence, are often referred to as poisons. This is reflected in the orders-of-magnitude variations reported in values for the exchange coefficient reported in the literature for nominally identical electrode materials[13,14,33]. To date, no descriptor, particularly with respect to surface additives, has been identified that can be utilized to predict the impact of surface additives on the surface exchange kinetics of different materials, and ultimately to optimize this kinetics for specific applications.

In this work, we demonstrate that the acidity of intentionally added insulating surface oxides can serve as the sought-after descriptor of the oxygen surface exchange rate on mixed ionic and electronic conductors. It is noteworthy to emphasize that a strategy of surface functionalization with insulating oxides goes against the conventional wisdom of strategies to improve surface exchange kinetics and therefore has not been seriously considered as a viable strategy. We selected praseodymium-doped ceria, $Pr_xCe_{1-x}O_{2-\delta}$, a model mixed conducting oxide with the fluorite crystal structure, to demonstrate this finding. First, we have a detailed understanding of its bulk defect equilibria and transport properties and, second, as a binary oxide it does not suffer from substantial segregation of one of the sublattice cations, as observed in the popular perovskites, such as (La,Sr)CoO_3, which suffers from selective Sr surface segregation. As recently reported by Schaube et al., the available literature data for surface exchange rates on nominally untreated $Pr_{0.1}Ce_{0.9}O_{2-\delta}$ spans over six orders of magnitude without a clear source identified for the spread[14]. The following work aims to understand the source of these wide swings in kinetics and provide insights on how they can be controlled and optimized.

Results

Acidity of binary oxides. Our approach is to study the influence of various oxides infiltrated onto the surface of a given mixed conductor, and relate their influence on the oxygen surface exchange kinetics to their respective acidity. The acidity of binary oxides can be expressed according to their tendency to accept an oxide ion. Following this principle, Smith constructed an acidity coefficient α, based on thermochemical data, that allows binary oxides to be placed on a scale, from strongly basic to strongly acidic[34]. An acidity scale for binary oxides, as proposed by Smith (some oxides have been removed for more clarity), is shown in Fig. 1.

$Pr_{0.1}Ce_{0.9}O_{2-\delta}$ further served well as a reference mixed conductor material because of its fast ionic conductivity, which ensures that bulk diffusion will not influence the determination of the oxygen chemical surface exchange coefficient k_{chem}. The exchange coefficient was measured by electrical conductivity relaxation on porous $Pr_{0.1}Ce_{0.9}O_{2-\delta}$ specimens[35] (measurements are detailed in Supplementary Note 3). The $Pr_{0.1}Ce_{0.9}O_{2-\delta}$ specimens were infiltrated by a series of binary oxides with Smith acidity values that ranged from strongly acidic to strongly basic. Five oxides were selected, which ranged from highly basic to highly acidic: Li_2O, CaO, Gd_2O_3, Al_2O_3 and SiO_2 (details on the selection of oxides are given in Supplementary Note 1).

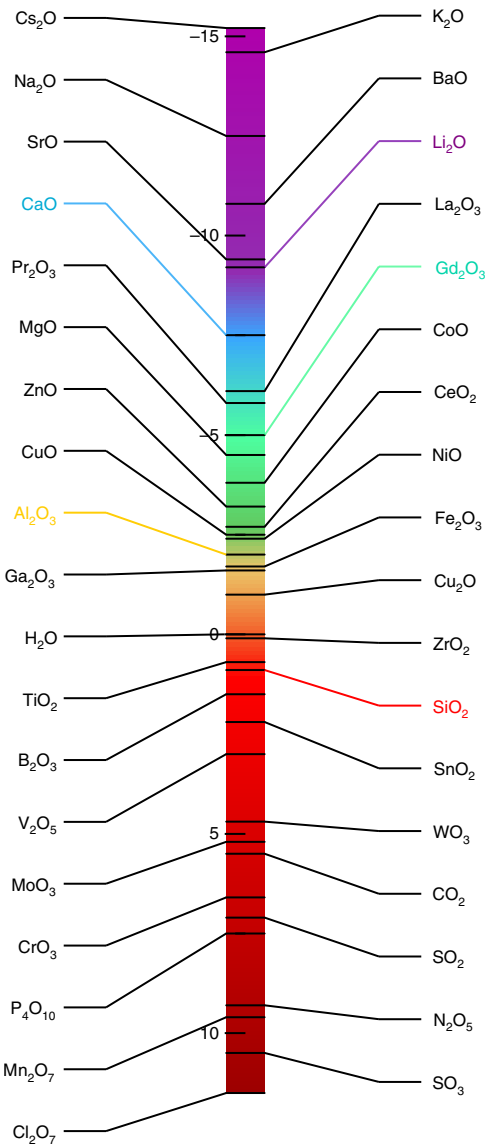

Fig. 1 | Acidity scale for binary oxides, as proposed by Smith[34]. H_2O is chosen as the origin—positive values are more acidic and negative values are more basic. The oxides with coloured text were infiltrated into $Pr_{0.1}Ce_{0.9}O_{2-\delta}$ in this study.

Microstructure analysis. Figure 2a shows the typical microstructure of the porous samples, with an average grain size of roughly 1 µm and a porosity (determined geometrically) of 26%. Figure 2b shows a high-angle annular dark-field-scanning transmission electron microscopy (TEM) image of a pore in a Gd_2O_3-infiltrated sample, taken as an example (for images and maps of other infiltrated samples, see Supplementary Note 2), along with elemental maps of Ce (Fig. 2c,e) and Gd (Fig. 2d,f) obtained by X-ray energy-dispersive spectrometry (XEDS). The maps show that the added oxides remain on the surface of the $Pr_{0.1}Ce_{0.9}O_{2-\delta}$ grains, with no sign of diffusion into the fluorite structure. The infiltration protocol yields rather large particles of roughly 100–200 nm, along with a more diffuse distribution of the element around the nanoparticles. This diffuse distribution does not appear to be continuous over the whole surface of $Pr_{0.1}Ce_{0.9}O_{2-\delta}$. A quick estimation of the surface coverage based only on the particle size gives a geometrical surface coverage of approximately 1.5–3% (a conformal and dense film

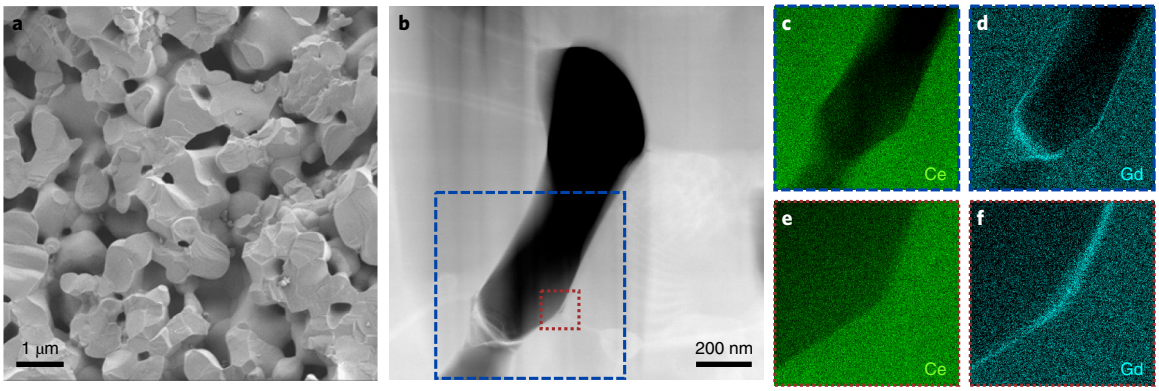

Fig. 2 | Microstructural analysis of the infiltrated porous $Pr_{0.1}Ce_{0.9}O_{2-\delta}$ samples. a, Cross-sectional scanning electron microscopy image of the Pr-doped ceria porous structure. **b**, High-angle annular dark-field-scanning TEM image of a pore in a Gd_2O_3-infiltrated sample, with elemental maps of Ce (**c**,**e**) and Gd (**d**,**f**) obtained by XEDS for selected areas indicated by the dashed blue and red lines in **b**. The blue frame is 700 × 700 nm² and the red frame is 130 × 130 nm².

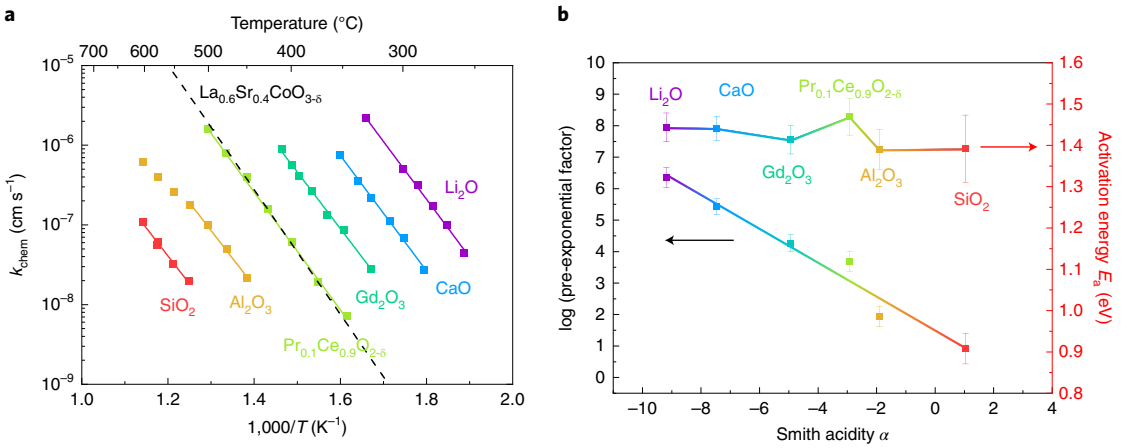

Fig. 3 | Oxygen surface exchange kinetics as a function of acidity. a, Oxygen chemical surface exchange coefficients of $Pr_{0.1}Ce_{0.9}O_{2-\delta}$ as a function of temperature for various surface modifications with selected binary oxides. Reference values for $La_{0.6}Sr_{0.4}CoO_{3-\delta}$ (black dashed line) are shown for comparison and taken from Egger et al.[37]. The error bars calculated from standard errors are smaller than the data points, and therefore are not represented. **b**, Pre-exponential factors and activation energies of k_{chem} as a function of the acidity factor. Error bars in **b** were calculated from the standard error of each linear fit presented in **a**.

would be approximately 2–9 nm thick, depending on the oxide). This means that most of the $Pr_{0.1}Ce_{0.9}O_{2-\delta}$ surface is free of those larger particles and accessible for molecular oxygen to react on its surface. Additionally, the surface area change induced by the infiltrated oxide is expected to be negligible. Although large particles are present on the surface, the infiltration process is expected to result in atomic dispersion of the added species over the whole surface, as observed, for example, for noble metals in sensors[36].

Oxygen surface exchange kinetics. The oxygen chemical surface exchange coefficients k_{chem} of both untreated $Pr_{0.1}Ce_{0.9}O_{2-\delta}$ specimens and those treated with the aforementioned additives (Li_2O, CaO, Gd_2O_3, Al_2O_3 and SiO_2) were derived from conductivity relaxation experiments (Supplementary Note 3). Figure 3a shows an Arrhenius plot of these results in the form of log k_{chem} versus 1,000/T plots, and includes literature values for $La_{0.6}Sr_{0.4}CoO_{3-\delta}$ (ref. [37]) for reference. There is an extremely strong dependence of the surface exchange kinetics on the nature of the binary oxides infiltrated onto the surface of the $Pr_{0.1}Ce_{0.9}O_{2-\delta}$ with values of k_{chem} that vary over nearly six orders of magnitude between SiO_2, the most acidic material investigated, and Li_2O, the most basic material investigated. Li_2O infiltration results in a nearly 1,000-fold increase in the oxygen chemical surface exchange coefficient as compared with the non-infiltrated $Pr_{0.1}Ce_{0.9}O_{2-\delta}$ reference, which enables equilibration of its oxygen stoichiometry with the atmosphere at temperatures as low as 260 °C in one hour. Additionally, a similar enhancement factor was confirmed with respect to the area specific resistance of $Pr_{0.1}Ce_{0.9}O_{2-\delta}$ thin films infiltrated with Li_2O, as measured by impedance spectroscopy (Supplementary Note 6). However, the highly acidic Al_2O_3 and SiO_2 led to 17- and 220-fold reductions in k_{chem}, respectively. Surprisingly, regardless of the direction of the change in k_{chem}, its activation energy remained rather constant within narrow limits.

Given the obvious dependence of $k_{chem} = A\exp(-E_a/k_BT)$ on the relative acidity of the infiltrated oxides, both the pre-exponential A and the activation energy E_a extracted from each of the curves in Fig. 3a are plotted in Fig. 3b as a function of the Smith acidity factor α. In the case of Al_2O_3, the points at a higher temperature tend to deviate from the linear fit, the source of which is presently not understood, but we suspect may be due to an experimental artefact.

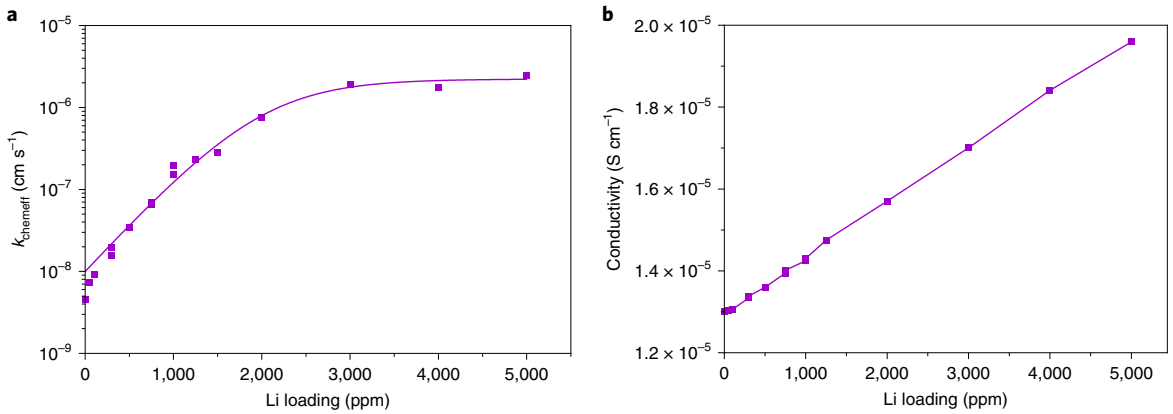

Fig. 4 | Li concentration dependence of exchange rate and electrical conductivity. a,**b**, Influence of the lithium loading amount on $k_{chemeff}$ (**a**) and conductivity (**b**), measured at 330 °C. The error bars calculated from standard errors are smaller than the data points, and therefore they are not represented. The solid lines through the data points serve only as guides to the eye.

As an α value is not available for $Pr_{0.1}Ce_{0.1}O_{2-\delta}$ (PCO) in the literature, we estimated it by taking an average between that of CeO_2 and Pr_2O_3, corrected for Pr concentration (10 at%), to yield $\alpha_{PCO} = -3.01$. This value was subsequently used as a reference value for comparison with those of other binary oxides utilized in this study. Remarkably, the activation energy was almost constant, centred above ~1.4 eV. As the variations are within the error bars over the whole range of α, it is difficult to draw any conclusion from this observed trend. The log of the pre-exponential factor A of k_{chem}, however, varies linearly, within experimental error, with the acidity of the infiltrated binary oxide. The roughly six orders of magnitude observed change in A is all the more impressive given the small level of infiltration loading. These results demonstrate how the acidity of surface-additive binary oxides, relative to that of their host, can serve as a descriptor to predict greatly enhanced or suppressed oxygen surface exchange kinetics of a mixed conducting oxide.

Influence of the concentration of infiltrated oxide on k_{chem}. To inquire if a minimum amount of infiltrated material is needed to trigger changes in oxygen surface exchange kinetics, the chemical surface exchange coefficient k_{chem} was measured for different loading levels of lithium oxide on $Pr_{0.1}Ce_{0.9}O_{2-\delta}$. A porous sample was infiltrated repeatedly with lithium nitrate to yield loadings that ranged from 50 to 5,000 ppm, and k_{chem} was measured at 330 °C between each infiltration step to determine its dependence on infiltration loading. As the transients changed their shapes for intermediate infiltration loading from a single time-constant exponential to a more complex shape, a different fitting procedure was used (Supplementary Note 4) and the calculated coefficient is called the effective exchange coefficient $k_{chemeff}$. Figure 4a demonstrates that lithium loadings as small as 50 ppm lead to improved values of $k_{chemeff}$ and that $k_{chemeff}$ continues to increase following each infiltration step, by as much as 2.5 orders of magnitude, up to a saturation value of around 3,000 ppm. These results demonstrate that by selecting the acidity and concentration of the infiltrated binary oxide, we can modify k_{chem} at will, and over six orders of magnitude, by following a simple experimental protocol. A similar trend, but in the opposite direction (degradation of k_{chem}), can also be observed with the infiltration of an acidic oxide like Cr_2O_3, for which a degradation of k_{chem} is observed with concentrations as low as 20 ppm (Supplementary Fig. 5). Further, as shown in Fig. 4b, the conductivity change induced by the addition of surface lithium oxide varies rather linearly with loading concentration, which suggests that the electron concentration at the surface of Pr-doped ceria has a direct and linear relationship with the concentration of lithium at the surface.

Conductivity and electronic structure. The trend of a systematic change in conductivity with surface additive observed for Li_2O in Fig. 4b is examined more broadly in Fig. 5a, which shows a systematic conductivity change, represented as the percentage change of the initial $Pr_{0.1}Ce_{0.9}O_{2-\delta}$ conductivity (remeasured on each sample prior to infiltration) as a function of the acidity of the infiltrated binary oxide. The conductivity increases with the addition to the surface of the more basic oxides, such as Li_2O, CaO and Gd_2O_3, but it decreases slightly under the $Pr_{0.1}Ce_{0.9}O_{2-\delta}$ baseline for the more acidic ones, such as Al_2O_3 and SiO_2. Given that only the near-surface conductivity of the $Pr_{0.1}Ce_{0.9}O_{2-\delta}$ specimens is expected to be enhanced and/or depressed by the surface additives (as shown by Raman analysis in Supplementary Note 9), the 10–25% observed increase in the overall effective conductivity with basic oxides must reflect much larger changes in electron concentration at or near the surface of the Pr-doped ceria. On the contrary, a depletion of electrons at the surface with acidic oxides should only lead to a small decrease in the overall conductivity given the short-circuiting character of the parallel conductive path through the much larger cross-section of the bulk. Broadly speaking, this enhancement and/or depletion of electrons at the surface is consistent with the Lewis theory that identifies bases as electron donors and acids as electron acceptors[38]. Lu et al.[39] demonstrated that the Pr valence state at the surface of Pr-doped ceria can deviate greatly from that of the bulk. A similar trend was also observed for near-surface $[Ce^{3+}] \equiv [e'_s]$, where $[e'_s]$ is the surface electron concentration, in undoped ceria[40]. To examine this possibility, the surfaces of the modified $Pr_{0.1}Ce_{0.9}O_{2-\delta}$ samples were analysed by photoelectron spectroscopy. No notable change in the Pr 3*d* and Ce 3*d* peaks were detected (spectra in the Supplementary Note 7). However Portier et al.[41] showed that the Smith acidity factor and the work function of the oxide are coupled, with the basic oxides having lower work functions than the acidic oxides. To verify this hypothesis, the work function of each sample was determined from X-ray photoelectron spectroscopy (XPS) measurements. The cutoff spectra were measured by applying a 10 eV pass energy, whereas the spectra for the Fermi energy (E_F) were collected applying a 50 eV pass energy. The work function values ϕ were obtained using the formula $\phi = h\nu - (E_{cutoff} - E_F)$; details about the procedures and spectra measured on each sample can be found in the Supplementary Note 7. Figure 5b shows the measured work function as a function of the acidity of the infiltrated binary oxide, which confirms the

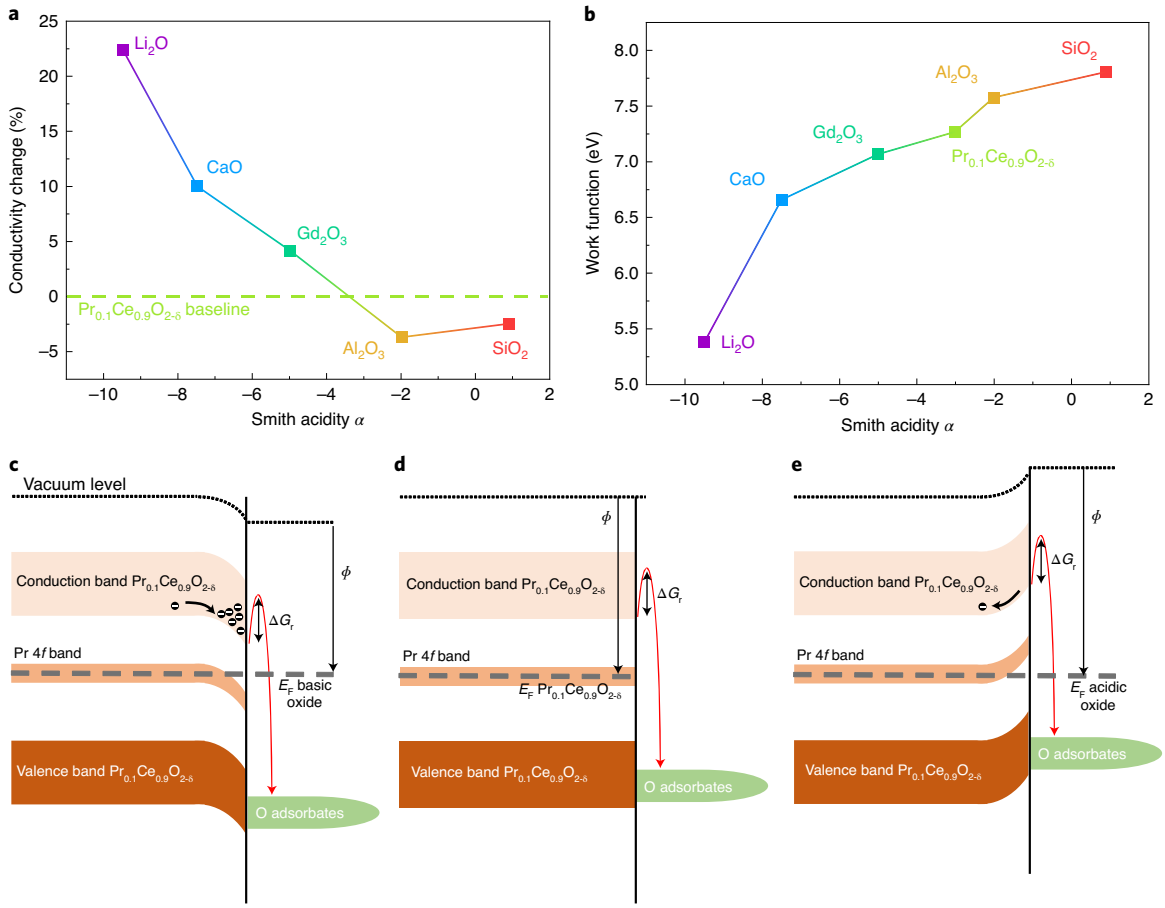

Fig. 5 | Conductivity and work-function dependence on acidity and the relation to electronic structure. a, Conductivity change (relative to the non-infiltrated Pr-doped ceria) as a function of the acidity factor of the infiltrated binary oxides, measured at 600 °C. **b**, Measured work function as a function of Smith acidity. **c**–**e**, Illustration of the effect of the acidity of the binary oxides on the band structure of Pr-doped ceria (**d**) for a basic oxide (**c**), such as Li_2O, and an acidic oxide (**e**), such as SiO_2. ΔG_r, Gibbs free energy for the oxygen exchange reaction; ϕ, work function of the sample.

trend proposed by Portier et al.[41]. As the changes in work function are greater than 2 eV, it is not likely to come from a displacement of the Fermi level of $Pr_{0.1}Ce_{0.9}O_{2-\delta}$ within the bandgap, especially as it is expected to be pinned within the narrow Pr 4*f* band[42]. We suggest rather that the measured work functions correspond to that of the infiltrated binary oxides and, given the geometry (porosity) and the biphasic character of the samples, these values should be viewed as a qualitative trend, rather than in a quantitative manner. In a non-degenerate semiconductor, such additives will cause a substantial band bending in the solid close to the gas interface, which leads to a substantial depletion or accumulation of charge carriers close to the surface, depending on the positions of their work functions relative to that of $Pr_{0.1}Ce_{0.9}O_{2-\delta}$, and thereby impacts the charge transfer reaction. Figure 5c–e gives a tentative illustration of the effect of the infiltrated oxide on the band structure of $Pr_{0.1}Ce_{0.9}O_{2-\delta}$: in the case of basic oxides, with a lower work function than that of $Pr_{0.1}Ce_{0.9}O_{2-\delta}$, the infiltration causes downward band bending of the $Pr_{0.1}Ce_{0.9}O_{2-\delta}$ bands and an accumulation of electrons at the surface. In the case of an acidic oxide, with a higher work function than that of $Pr_{0.1}Ce_{0.9}O_{2-\delta}$, infiltration causes an upward band bending of the $Pr_{0.1}Ce_{0.9}O_{2-\delta}$ bands, and thus depletes electrons at the surface. The activation energy does not change given that the energy needed to transfer an electron from the $Pr_{0.1}Ce_{0.9}O_{2-\delta}$ surface to the adsorbate remains independent of the surface electron concentration, which agrees with the proposal of De Souza[43]. To examine this finding with regard to acidity as a more general descriptor of oxygen exchange kinetics in mixed conductors, we tested it in a preliminary manner with the popular perovskite cathode $La_{0.6}Sr_{0.4}CoO_{3-\delta}$. Indeed, we obtained the same trend of k_{chem} variation with Li or Al infiltration (Supplementary Note 8), which highlights the broader utility of investigating the acid–base behaviour of additive binary oxides, and the great potential of this approach to improve oxygen exchange kinetics.

Discussion

It is useful to estimate the change of surface electron concentration depending on the infiltrated binary oxide. Based on the expression proposed by Guo and Waser[44] and a dielectric constant of 35 (ref. [45]), a typical width of the space charge for heavily doped ceria should extend to ~2 nm, which means that total measured changes in the overall sample conductivity (Figs. 4b and 5a) would reflect orders-of-magnitude changes in the surface conductivity, and therefore, presumably, in the surface electron concentration. According to De Souza[43], the surface exchange coefficient and the surface electron concentration are directly related. In Supplementary Note 5, we describe the calculation of surface electron concentrations from the pre-exponential factors of *k*. The surface electron concentrations were also estimated from the conductivity changes observed in Fig. 5a, based on a simple model of two parallel resistive pathways, that is, a bulk path and a surface path, the latter 2 nm thick, according to the estimated width of the space charge. Comparison of the surface electron concentration (and conductivity) calculated

from both methods shows that the calculation derived from the pre-exponential of k^* overestimates [e] as compared with that calculated from the more direct conductivity change measurements. The latter, although they clearly point to a nearly two orders of magnitude change in surface electron concentration and surface conductivity, are insufficient to account for the wide span in the measured surface exchange coefficient values. As the apparent change in surface electron concentration with acidity in itself does not suffice to account for the changes in the surface exchange coefficient, we hypothesize that the electron density may have an indirect effect on k_{chem} beyond just serving as a reactant for the charge transfer reaction. Moreover, Chen et al.[18] recently showed results that point to the adsorption of neutral oxygen as the rate-determining step for oxygen exchange in Pr-doped ceria, which is in direct conflict with the model proposed by De Souza[43]. The question of how changes in the surface electron concentration impact the oxygen exchange kinetics therefore remains open, and needs further investigation. Another feature to consider is why the overall conductivity changes substantially with the addition of the infiltrated oxides, even though the oxides are seen as relative dilute discrete particles, as observed by TEM (Fig. 2). The results suggest that the effect of the additives are not limited to the particles or their triple-phase boundaries with the PCO and gas phase, but rather extend beyond the particles to enhance the electron concentration at the seemingly free $Pr_{0.1}Ce_{0.9}O_{2-\delta}$ surface. A reasonable working hypothesis is that, although the infiltrated phase forms large particles with little direct evidence of a conformal coating, the surrounding and adjacent PCO surface also becomes coated by particles near to atomic size, which extends the effect of the infiltration beyond the visible particles. This is a common understanding in the sensor field where catalysts are infiltrated onto sensor surfaces to achieve an enhanced sensitivity over nearly the full surface of the sensor[36].

Other effects linked to the acidity of the infiltrated binary oxides, in addition to their impact on the surface electron concentration, could also come into play. As the acidity of an oxide is also related to its chemical hardness[41], the infiltrated oxide could also have an influence on the Pr–O and Ce–O bond strengths, which in turn could modify the surface exchange kinetics. The more basic oxides, such as Li_2O and CaO, are also known to form peroxide bonds with an additional oxygen, and therefore change the oxygen oxidation state from −2 to −1, which could also impact the overall oxygen surface exchange rate constant of $Pr_{0.1}Ce_{0.9}O_{2-\delta}$, as suggested previously for $SrTiO_3$ (refs [27,28]).

Overall, this points to the need for future more detailed studies that focus on achieving an improved understanding of how, in detail, the acidity of binary oxides impacts the oxygen exchange kinetics of mixed conducting oxides.

Having identified the connection between the acidity of surface oxides and oxygen exchange kinetics, it may now be possible to better understand poisoning effects in solid oxide fuel cells. Indeed, most of the well-known poisons for oxygen electrodes, namely CrO_3, SO_2 and SiO_2, are quite acidic. Although the degradation in performance is often attributed to these oxides serving to mask active sites, a better explanation, based on the results reported here, focuses instead on their contribution to the depletion of surface electron concentrations by the electrochemical potential or E_F alignment. This further explains the reported enhancements of k_{chem}, such as La on Pr-doped ceria[46], strontium carbonate on lanthanum strontium cobalt ferrite[25] or SrO or BaO on Fe-doped strontium titanate[27,28].

Moreover, these results bring insights towards explaining the source of the wide range of k_{chem} values (over six orders of magnitude) measured for nominally untreated $Pr_{0.1}Ce_{0.9}O_{2-\delta}$ and reported in the literature[14]. Most of the protocols used to prepare oxide materials involve grinding steps, which can be done in agate or alumina mortars, or by ball milling with ZrO_2 balls, which are all acidic and could induce poisoning of the surface. However, many research groups also working with Li- or Na-based batteries might see enhancements in k_{chem} that could come from Li or Na cross-contamination.

This acid–base approach also reveals that the oxygen exchange kinetics are only partially dependent on the bulk properties of the material (provided that the vacancy concentration is reasonably high). This suggests that we could expect a greater flexibility in identifying new active catalysts, ideally largely composed of non-critical elements. Mixed conductors with poor initial oxygen exchange kinetics, but composed of non-critical elements, could potentially be activated through the infiltration of inexpensive and abundant basic oxides, such as CaO or even Na_2O.

Using the basicity as a descriptor to improve reaction kinetics could also be extended to other reactions and other fields of research. For example, basic centres can improve the kinetics of N_2 reduction for the Haber–Bosh process[47], or improve the sensitivity of sensors for ethanol detection[48]. Although this effect has been observed, this formalism using the Smith acidity factor could help those different communities define more precise strategies to investigate new materials in a number of other fields that involve the surfaces of mixed conducting metal oxides.

In summary, the role of the acidity of surface-infiltrated binary oxides on the oxygen exchange rate k_{chem} of mixed conducting $Pr_{0.1}Ce_{0.9}O_{2-\delta}$ was examined and found to be an extremely sensitive descriptor of those kinetics. Variations in k_{chem} by nearly six orders of magnitude could be reproducibly induced by selecting the acidity of one of five binary oxides used for infiltration, which range from the lowest k_{chem} value for the most acidic (SiO_2) to the highest k_{chem} value for the most basic (Li_2O) of the oxides, with the impact of acidity largely limited to the pre-exponential term for k_{chem}. Lithia loadings as small as 50 ppm led to improved values of $k_{chemeff}$ and continued to increase with systematic infiltration steps by as much as 2.5 orders of magnitude, up to a saturation value of 3,000 ppm. Similar preliminary studies on $La_{0.6}Sr_{0.4}CoO_{3-\delta}$ showed a similar impact of the relative acidity of infiltrated binary oxides on k_{chem}. Increases in k_{chem} were further correlated with increases in the electrical conductivity of $Pr_{0.1}Ce_{0.9}O_{2-\delta}$ and lower surface work functions for the infiltrated specimens with more basic oxides than $Pr_{0.1}Ce_{0.9}O_{2-\delta}$ and with decreases in the electrical conductivity of the $Pr_{0.1}Ce_{0.9}O_{2-\delta}$ and higher surface work functions for the infiltrated specimens with more acidic oxides than $Pr_{0.1}Ce_{0.9}O_{2-\delta}$. These observations suggest that the relative acidity of the infiltrated oxides impacts e'_s and, in turn, the oxygen exchange reaction. Further studies to confirm this hypothesis are indicated as well as to establish the influence of acidity on surface oxygen adsorptivity.

The discovery of the acidity of infiltrated oxides as a descriptor of k_{chem} can be expected to lead to important improvements in devices such as solid oxide fuel cells, and also help to understand the effects of major surface poisons in these systems. One can thus expect to recover performance loss that results from the degradation due to surface poisoning by acidic oxides by a subsequent treatment with more basic oxides. We expect that the use of basicity as a descriptor to improve reaction kinetics could also be extended to other reactions and other fields of research.

Methods

Sample preparation. The $Pr_{0.1}Ce_{0.9}O_{2-\delta}$ powders were synthesized by a solid-state route, that is, by ball milling a mixture of CeO_2 (99.99% purity, Alfa Aesar) and Pr_6O_{11} (99.9% purity, Sigma Aldrich) with ZrO_2 balls in EtOH overnight, pressing the mixed powder into a pellet and annealing it at 1,400 °C for 6 h. Two more steps of ball milling, pressing and annealing at 1,400 °C followed to produce a powder with a more homogeneous grain size.

The bar samples ($20 \times 5 \times 1$ mm^3) for conductivity relaxation measurements were all prepared from the same powder batch, with specimens pressed into 30-mm-diameter pellets and sintered at 1,450 °C for 1 h. All the samples were then cut from the same pellet with a diamond saw to ensure that they all had the

same composition and microstructure. The oxides were added to the surface of $Pr_{0.1}Ce_{0.9}O_{2-\delta}$ by the infiltration of a 0.2 M solution of the nitrate of each cation (except for SiO_2, for which tetraethylorthosilicate was used), and the infiltrated volume adapted to reach a precise loading of 0.5 at% (5,000 ppm). Additionally, Li_2O was infiltrated with loadings that ranged from 50 to 5,000 ppm to study the effect of loading level on k_{chem}. All the samples were first measured without infiltration to ensure that the reference chemical surface exchange coefficient remained constant for all the samples. The infiltrated materials were then calcined in situ at 600 °C for 1 h prior to the relaxation measurements.

Conductivity relaxation measurements. Four wires were wrapped around the bar sample and contacted with gold paste. The conductivity measurements are done with a HP3478A digital multimetre in a four-wire resistance measurement mode. The p_{O_2} steps applied to the samples were from 0.1 to 0.2 atm, controlled with two mass-flow controllers that mixed ultrahigh purity nitrogen and oxygen (grade 5.0, Airgas). First, the samples were all measured prior to infiltration, to establish their initial k_{chem} (Supplementary Fig. 2h). The standard deviation calculated from the initial k_{chem} values is ±3.3 %. The samples were then infiltrated with a nitrate solution (or tetraethyl orthosilicate) of the corresponding cation dissolved in ethanol to a concentration of 0.2 M. The samples were ~0.65 g and were infiltrated with ~100 µl of solution. The infiltration was performed on the sample hanging onto the measurement wires so that the entire volume of solution remained inside the porous sample without dripping elsewhere, which therefore increased the precision and repeatability of the infiltration loading. The infiltrated phase was then calcined in situ under synthetic air at 600 °C for 1 h with a heating ramp rate of 5 °C min^{-1}.

XPS measurements. XPS (Thermo Scientific K-Alpha, XPS instrument) was performed to investigate the chemical composition of the $Pr_{0.1}Ce_{0.9}O_{2-\delta}$ samples. The monochromatic Al Kα X-ray source (1,486.6 eV) with a 400 mm spot size was operated at of 200 eV for the survey scan, and narrow scan spectra were recorded at a pass energy of 50 eV. The K-Alpha charge compensation system was applied to prevent localized charge build-up during the analysis, using 5 eV electrons and low-energy Ar ions. The binding-energy scale was calibrated on the neutral carbon set at 284.8 eV. The recorded spectra were processed by Avantage software using a peak-fitting routine with Shirley background and symmetrical 70–30% mixed Gaussian–Lorentzian peak shapes.

TEM measurements. Thin lamellae of the bar samples were prepared for TEM using a dual-beam focused ion beam scanning electron microscope (Helios Nanolab 600i, FEI Company) with the 'lift-out' technique. Prior to this, the bar samples were infiltrated with a two-part epoxy under vacuum to protect the porous surface and coated in Au using sputter deposition to prevent charging. Thin sections were prepared and thinned at 30 kV, followed by additional thinning at 5 and 2 kV to reduce amorphous damage. Imaging and XEDS mapping were carried out on a TEM with a Cs corrector on both the probe-forming and image-forming lenses, a SSD XEDS detector and either a thermal or cold field-emission gun operated at 200 keV (JEM-200F or JEM-200CF, JEOL Ltd).

Data availability

The datasets of conductivity relaxation analysed during the current study are available in the source files of this manuscript. All other data are available within the paper and its Supplementary Information files. Source data are provided with this paper.

Received: 6 March 2020; Accepted: 2 September 2020;
Published online: 05 October 2020

References

1. Chueh, W. C. et al. High-flux solar-driven thermochemical dissociation of CO_2 and H_2O using nonstoichiometric ceria. *Science* **330**, 1797–1801 (2010).
2. Kilner, J. A. & Burriel, M. Materials for intermediate-temperature solid-oxide fuel cells. *Annu. Rev. Mater. Res.* **44**, 365–393 (2014).
3. Laguna-Bercero, M. A. Recent advances in high temperature electrolysis using solid oxide fuel cells: a review. *J. Power Sources* **203**, 4–16 (2012).
4. Wei, Y., Yang, W., Caro, J. & Wang, H. Dense ceramic oxygen permeable membranes and catalytic membrane reactors. *Chem. Eng. J.* **220**, 185–203 (2013).
5. Whittingham, M. S. Lithium batteries and cathode materials. *Chem. Rev.* **104**, 4271–4301 (2004).
6. Montini, T., Melchionna, M., Monai, M. & Fornasiero, P. Fundamentals and catalytic applications of CeO_2-based materials. *Chem. Rev.* **116**, 5987–6041 (2016).
7. Wang, C., Yin, L., Zhang, L., Xiang, D. & Gao, R. Metal oxide gas sensors: sensitivity and influencing factors. *Sensors* **10**, 2088–2106 (2010).
8. Barsan, N., Koziej, D. & Weimar, U. Metal oxide-based gas sensor research: how to? *Sens. Actuators B* **121**, 18–35 (2007).
9. Jeong, D. S. et al. Emerging memories: resistive switching mechanisms and current status. *Rep. Prog. Phys.* **75**, 076502 (2012).
10. Akinaga, H. & Shima, H. Resistive random access memory (ReRAM) based on metal oxides. *Proc. IEEE* **98**, 2237–2251 (2010).
11. Adler, S. B. Factors governing oxygen reduction in solid oxide fuel cell cathodes. *Chem. Rev.* **104**, 4791–4843 (2004).
12. Gao, Z., Mogni, L. V., Miller, E. C., Railsback, J. G. & Barnett, S. A. A perspective on low-temperature solid oxide fuel cells. *Energy Environ. Sci.* **9**, 1602–1644 (2016).
13. Rupp, G. M., Kubicek, M., Opitz, A. K. & Fleig, J. In situ impedance analysis of oxygen exchange on growing $La_{0.6}Sr_{0.4}CoO_{3-\delta}$ thin films. *ACS Appl. Energy Mater.* **1**, 4522–4535 (2018).
14. Schaube, M., Merkle, R. & Maier, J. Oxygen exchange kinetics on systematically doped ceria: a pulsed isotope exchange study. *J. Mater. Chem. A* **7**, 21854–21866 (2019).
15. Kubicek, M., Limbeck, A., Frömling, T., Hutter, H. & Fleig, J. Relationship between cation segregation and the electrochemical oxygen reduction kinetics of $La_{0.6}Sr_{0.4}CoO_{3-\delta}$ thin film electrodes. *J. Electrochem. Soc.* **158**, B727–B734 (2011).
16. Yokokawa, H., Tu, H., Iwanschitz, B. & Mai, A. Fundamental mechanisms limiting solid oxide fuel cell durability. *J. Power Sources* **182**, 400–412 (2008).
17. Perry, N. H. & Ishihara, T. Roles of bulk and surface chemistry in the oxygen exchange kinetics and related properties of mixed conducting perovskite oxide electrodes. *Materials* **9**, 858 (2016).
18. Chen, D. et al. Constructing a pathway for mixed ion and electron transfer reactions for O_2 incorporation in $Pr_{0.1}Ce_{0.9}O_{2-x}$. *Nat. Catal.* **3**, 116–124 (2020).
19. Cao, Y., Gadre, M. J., Ngo, A. T., Adler, S. B. & Morgan, D. D. Factors controlling surface oxygen exchange in oxides. *Nat. Commun.* **10**, 1346 (2019).
20. Wang, L., Merkle, R., Mastrikov, Y. A., Kotomin, E. A. & Maier, J. Oxygen exchange kinetics on solid oxide fuel cell cathode materials—general trends and their mechanistic interpretation. *J. Mater. Res.* **27**, 2000–2008 (2012).
21. Jung, W. C. & Tuller, H. L. A new model describing solid oxide fuel cell cathode kinetics: model thin film $SrTi_{1-x}Fe_xO_{3-\delta}$ mixed conducting oxides—a case study. *Adv. Energy Mater.* **1**, 1184–1191 (2011).
22. Jung, W. & Tuller, H. L. Investigation of surface Sr segregation in model thin film solid oxide fuel cell perovskite electrodes. *Energy Environ. Sci.* **5**, 5370–5378 (2012).
23. Opitz, A. K. et al. The chemical evolution of the $La_{0.6}Sr_{0.4}CoO_{3-\delta}$ surface under SOFC operating conditions and its implications for electrochemical oxygen exchange activity. *Top. Catal.* **61**, 2129–2141 (2018).
24. Rupp, G. M., Opitz, A. K., Nenning, A., Limbeck, A. & Fleig, J. Real-time impedance monitoring of oxygen reduction during surface modification of thin film cathodes. *Nat. Mater.* **16**, 640–645 (2017).
25. Li, M. et al. Mechanism for the enhanced oxygen reduction reaction of $La_{0.6}Sr_{0.4}Co_{0.2}Fe_{0.8}O_{3-\delta}$ by strontium carbonate. *Phys. Chem. Chem. Phys.* **19**, 503–509 (2017).
26. Mutoro, E., Crumlin, E. J., Biegalski, M. D., Christen, H. M. & Shao-Horn, Y. Enhanced oxygen reduction activity on surface-decorated perovskite thin films for solid oxide fuel cells. *Energy Environ. Sci.* **4**, 3689–3696 (2011).
27. Wagner, S. F. et al. Enhancement of oxygen surface kinetics of $SrTiO_3$ by alkaline earth metal oxides. *Solid State Ion.* **177**, 1607–1612 (2006).
28. Argirusis, C. et al. Enhancement of oxygen surface exchange kinetics of $SrTiO_3$ by alkaline earth metal oxides. *Phys. Chem. Chem. Phys.* **7**, 3523–3525 (2005).
29. Cheng, Y. et al. Enhancing oxygen exchange activity by tailoring perovskite surfaces. *J. Phys. Chem. Lett.* **10**, 4082–4088 (2019).
30. Paige, J. M. et al. Surface modification of SOFC cathodes by Co, Ni, and Pd oxides. *Solid State Ion.* **341**, 115051 (2019).
31. Tsvetkov, N., Lu, Q., Sun, L., Crumlin, E. J. & Yildiz, B. Improved chemical and electrochemical stability of perovskite oxides with less reducible cations at the surface. *Nat. Mater.* **15**, 1010–1016 (2016).
32. Sasaki, K. et al. Chemical durability of solid oxide fuel cells: influence of impurities on long-term performance. *J. Power Sources* **196**, 9130–9140 (2011).
33. Chen, T., Harrington, G. F., Masood, J., Sasaki, K. & Perry, N. H. Emergence of rapid oxygen surface exchange kinetics during in situ crystallization of mixed conducting thin film oxides. *ACS Appl. Mater. Interfaces* **11**, 9102–9116 (2019).
34. Smith, D. W. An acidity scale for binary oxides. *J. Chem. Educ.* **64**, 480–481 (1987).
35. Ganeshananthan, R. & Virkar, A. V. Measurement of surface exchange coefficient on porous $La_{0.6}Sr_{0.4}CoO_{3-\delta}$ samples by conductivity relaxation. *J. Electrochem. Soc.* **152**, A1620–A1628 (2005).
36. Cabot, A. et al. Analysis of the noble metal catalytic additives introduced by impregnation of as obtained SnO_2 sol–gel nanocrystals for gas sensors. *Sens. Actuators B* **70**, 87–100 (2000).
37. Egger, A., Bucher, E., Yang, M. & Sitte, W. Comparison of oxygen exchange kinetics of the IT-SOFC cathode materials $La_{0.5}Sr_{0.5}CoO_{3-\delta}$ and $La_{0.6}Sr_{0.4}CoO_{3-\delta}$. *Solid State Ion.* **225**, 55–60 (2012).

38. Miessler, G. L., Fischer, P. J. & Tarr, D. A. *Inorganic Chemistry* (Pearson, 1991).
39. Lu, Q. et al. Surface defect chemistry and electronic structure of $Pr_{0.1}Ce_{0.9}O_{2-\delta}$ revealed in operando. *Chem. Mater.* **30**, 2600–2606 (2018).
40. Chueh, W. C. et al. Highly enhanced concentration and stability of reactive Ce^{3+} on doped CeO_2 surface revealed in operando. *Chem. Mater.* **24**, 1876–1882 (2012).
41. Portier, J., Poizot, P., Tarascon, J.-M., Campet, G. & Subramanian, M. A. Acid–base behavior of oxides and their electronic structure. *Solid State Sci.* **5**, 695–699 (2003).
42. Bishop, S. R., Stefanik, T. S. & Tuller, H. L. Defects and transport in $Pr_xCe_{1-x}O_{2-\delta}$: composition trends. *J. Mater. Res.* **27**, 2009–2016 (2012).
43. De Souza, R. A. Limits to the rate of oxygen transport in mixed-conducting oxides. *J. Mater. Chem. A* **5**, 20334–20350 (2017).
44. Guo, X. & Waser, R. Electrical properties of the grain boundaries of oxygen ion conductors: acceptor-doped zirconia and ceria. *Prog. Mater. Sci.* **51**, 151–210 (2006).
45. Mebane, D. S. & De Souza, R. A. A generalised space–charge theory for extended defects in oxygen-ion conducting electrolytes: from dilute to concentrated solid solutions. *Energy Environ. Sci.* **8**, 2935–2940 (2015).
46. Zhao, L., Perry, N. H., Daio, T., Sasaki, K. & Bishop, S. R. Improving the Si impurity tolerance of $Pr_{0.1}Ce_{0.9}O_{2-\delta}$ SOFC electrodes with reactive surface additives. *Chem. Mater.* **27**, 3065–3070 (2015).
47. Grubel, K., Brennessel, W. W., Mercado, B. Q. & Holland, P. L. Alkali metal control over N–N cleavage in iron complexes. *J. Am. Chem. Soc.* **136**, 16807–16816 (2014).
48. Jinkawa, T., Sakai, G., Tamaki, J., Miura, N. & Yamazoe, N. Relationship between ethanol gas sensitivity and surface catalytic property of tin oxide sensors modified with acidic or basic oxides. *J. Mol. Catal. A* **155**, 193–200 (2000).

Acknowledgements

This research was primarily supported by the US Department of Energy (DOE), National Energy Technology Laboratory (NETL), Office of Fossil Energy under Award no. DE-FE0031668—Self-Regulating Surface Chemistry for More Robust Highly Durable Solid Oxide Fuel Cell Cathodes. Supplementary support was provided by the US DOE, Office of Science, Basic Energy Sciences (BES), under Award no. DE-SC0002633—Chemomechanics of Far-From-Equilibrium Interfaces (XPS studies). G.F.H. acknowledges support from a Kakenhi Grant-in-Aid for Encouragement of Young Scientists (B) Award (no. JP18K13992) (TEM studies). Thanks go to A. Grimaud and D. Kalaev for helpful discussions.

Author contributions

C.N. suggested the original idea. C.N. and H.L.T. designed the experimental protocol. C.N. prepared the samples, built the experimental set-up and performed the conductivity relaxation measurements. G.F.H. prepared the lamellae for TEM, performed the TEM measurements and computed the defect model used to interpret the results. C.T. prepared and measured the samples by XPS. C.T. and B.Y. performed the analysis of the XPS measurements and interpreted the results. T.D. performed the Raman spectroscopy measurements and interpreted the results. H.L.T. supervised the work and provided guidance throughout the project. C.N. and H.L.T. wrote the manuscript. All the co-authors discussed the results and helped to revise the manuscript.

Competing interests

The authors declare no competing interests.

Additional information

Supplementary information is available for this paper at https://doi.org/10.1038/s41929-020-00520-x.

Correspondence and requests for materials should be addressed to C.N.

Reprints and permissions information is available at www.nature.com/reprints.

Publisher's note Springer Nature remains neutral with regard to jurisdictional claims in published maps and institutional affiliations.